# Study of Negative Electron Affinity GaAs Photocathodes

Brian S. Henderson
*Department of Physics and Astronomy,*
*Rice University, Houston, Texas, 77005*
(Dated: August 7, 2009)

The proposed Energy Recovery Linac (ERL) at Cornell University and other future accelerator projects will depend on photocathodes to produce high-brightness electron beams while maintaining high quantum efficiency over extended periods of time. This paper presents a two-part study of the activation and characteristics of the emission of negative electron affinity GaAs photocathodes. New methods of photocathode activation were explored and characterized and preliminary work was completed in the design of a device with the capability to measure the two-dimensional energy distribution of electron beams produced by photocathodes.

## I. INTRODUCTION

Semiconductor III-V photocathodes activated to negative electron affinity (NEA) serve as electron beam sources for many applications including large-scale accelerator projects, electron lithography, and night vision. Photocathodes consisting of a p-doped GaAs crystal activated by depositing a few monolayers of cesium and a strong oxidizer, such as fluorine or oxygen, on the crystal surface have been shown repeatedly to produce strong electron beams when illuminated with laser light over a broad range of wavelengths [1]. It is desirable to produce photocathodes with high quantum efficiency and long lifetime, both of which depend on the interactions at the photocathode surface developed during cathode activation.

Electron affinity ($\chi$) is defined as the potential barrier that an electron at the conduction band minimum energy ($E_{cb}$) of a cathode must overcome to escape into the vacuum level ($E_{vac}$). By p-doping a GaAs crystal, the Fermi level ($E_F$) of the system is lowered towards the valence band maximum of the crystal ($E_{vb}$) [2]. The strong dipole field created near the surface of the crystal by the deposition of cesium and the oxidizer lowers $E_{vac}$ below $E_{cb}$, thus resulting in a work function $\varphi$ that is less than the gap between $E_{vb}$ and $E_{cb}$. To maintain equilibrium at this surface, the valence and conduction bands must bend downwards ($V_{bb}$) while the Fermi level is unaffected. Hence, for electrons in the bulk of the crystal, away from the surface, the effective electron affinity ($\chi_{eff}$) is negative favoring electrons leaving the crystal into the vacuum when energetic photons strike the crystal (see Figure 1).

The quality of a photocathode may be expressed in terms of two essential parameters. The quantum efficiency (QE) of a cathode is defined to be the ratio of the number of electrons produced by the cathode to the number of incident photons. Thus, for incident laser power $P$ at wavelength $\lambda$ incident on the crystal producing photocurrent $I_p$ is:

$$\mathrm{QE} = \left| \frac{hcI_p}{P\lambda e} \right| \cdot 100\% \tag{1}$$

where $h$ is Planck's constant, $c$ the speed of light, and $e$ the elementary charge. As shown, QE is customarily quoted as a percent value.

The second factor of merit is the span of time over which an activated cathode continues to produce a satisfactory QE. Two different cathode lifetimes are relevant: the operational

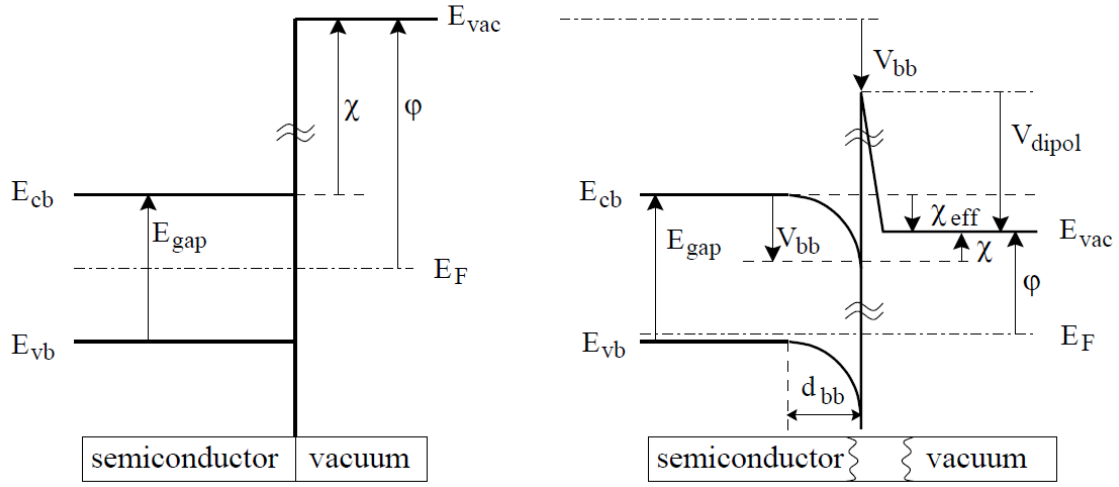


FIG. 1: Energy diagrams of the interface between crystal and vacuum for an unaltered GaAs crystal (left) and a p-doped GaAs crystal activated to achieve negative electron affinity (right) [3].

lifetime under high current production conditions and the "dark" lifetime measured at very low laser power which depends on the interactions and rearrangement processes on the surface of the cathode. For the purposes of the this paper only dark lifetimes are considered. The "simple" lifetime is defined to be the time required for the QE of an activated cathode to drop by a factor of $1/e$ (.368). In several instances, the concept of an "instantaneous lifetime" is used. In this case, the lifetime is the time that would be required for the QE to drop by a factor of $1/e$ if it is assumed that the QE will continue to decay exponentially from its present state.

The purpose of the first part of this study was to test several traditional and new methods of photocathode activation and characterize the methods in terms of the aforementioned figures of merit as well as examining the interactions and structure of the photocathode surface induced by each activation method. The second part of the study focused on the preliminary development of a device that will allow the measurement of both the transverse and longitudinal energies distributions of electrons emitted by a photocathode. Currently, methods exist for measuring one of the energy distribution dimensions at a time. Since the maximum brightness of an electron beam produced by a photocathode is dependent on the transverse energy and the longitudinal energy distribution of electrons provides valuable insight into the physics of photoemission from the cathode [4], it is highly advantageous to develop methods which allow the examination of both dimensions simultaneously. Preliminary work was completed in the design of such a device, following the methods developed by Orlov, et al [5].

## II. STUDY OF PHOTOCATHODE ACTIVATION

Activations of GaAs photocathodes were conducted using cesium and several different oxidizing compounds, including the commonly-used oxidizer $NF_3$ and new compounds $XeF_2$ and pure molecular nitrogen. The primary goal was to characterize the activation and

decay behaviors of the quantum efficiency for each oxidizer with the intent of maximizing cathode stability and lifetime. Of particular interest was the role of nitrogen, introduced by either the oxidizing compound or other sources, in the interactions on the surface of the photocathode. Provided for reference is a brief summary of the current status of GaAs photocathode development. A description of the experimental setup and methods and the results and analysis of the activations conducted during the study follow.

## A. Background

While Albert Einstein proposed his quantum theory of photoemission in 1903, which described the process of electron emission from photocathodes as primarily a surface effect, it was not until 1958 when W.E. Spicer more comprehensively described photoemission as a bulk process instead [6]. Spicer described photoemission as a three step process: the absorption of the incident photon within the bulk of the cathode resulting in the excitation of an electron to the conduction band, the transport of the excited electron to the cathode surface, and the release of the electron from the surface into the vacuum.

P-doped gallium arsenide, activated with a layer of cesium, was first proposed as a good candidate for the development of NEA photocathodes by Scheer and van Laar in 1965 [7]. Furthermore, Scheer and van Laar found that exposing the atomically clean GaAs surface to both cesium and oxygen created a more effective photoemitter with a broad range of possible applications. The development of polarized electron beams for use in linear accelerators led to the use of nitrogen trifluoride as the oxidizing agent for photocathodes [8]. The use of $NF_3$ was claimed to be easier to conduct activations with than oxygen by some groups and was believed to provide a simpler cathode surface structure consisting of Cs-F dipoles [9]. While many models have been proposed for the surface interactions associated with photocathode activation, the process is still poorly understood.

Currently, there is strong interest in developing photocathodes that produced "cold" DC electron beams, i.e. beams that are mono-energetic and have small transverse energy spreads [10]. Motivated by this, there has been significant work in attempts to measure both the transverse and longitudinal energy distributions of electrons beams produced by different cathode activations [1–3]. The work of Hoppe, et al has produced the first device capable of simultaneous measurement of the transverse and longitudinal energy distributions. Complete knowledge of the energies of electrons produced by photocathodes would be extremely beneficial in determining the cathode surface interactions and structures responsible for activation to NEA.

## B. Methods

### *1. Experimental Setup*

The photocathode activations were conducted using the setup shown in Figure 2. The chamber containing the photocathode was kept at ultra-high vacuum ($< 10^{-10}$ Torr) using an ion pump system to maintain a clean and controlled environment. The GaAs cathode, a thin wafer approximately 2 cm in diameter, was mounted to a holder which was in turn connected to a heater which could be used to control the temperature of the cathode.

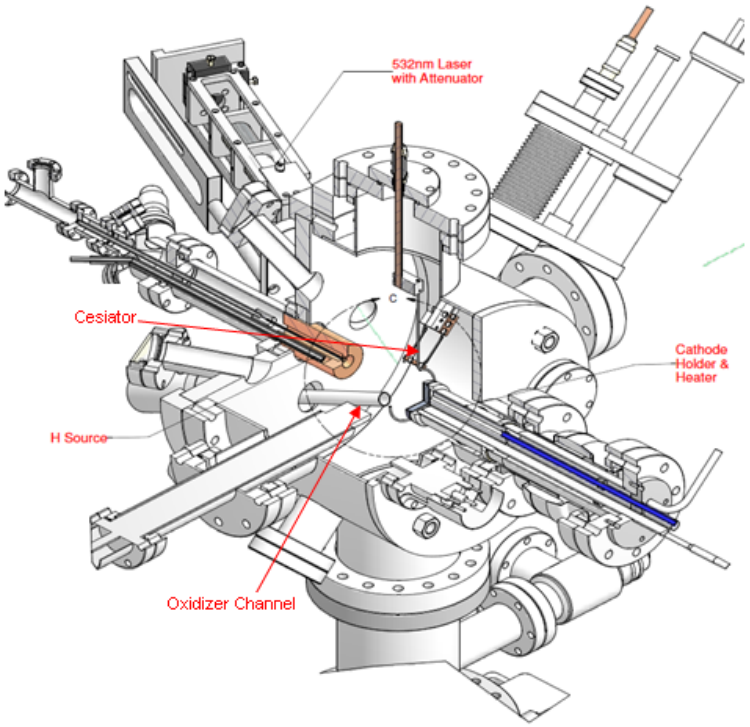


FIG. 2: Schematic of the chamber used for photocathode activations and QE/lifetime measurements.

A 532 nm laser was used to illuminate the cathode in "reflection mode", i.e. the laser was shone onto the side of the crystal from which electrons were to be emitted. The laser power was monitored using a laser power meter monitoring the reflected light from the cathode, which was in turn calibrated with the direct output of the laser. In the activations conducted for this study, a relatively low, constant laser power (approximately 30 $\mu$W) was maintained throughout activation and decay measurements except where otherwise noted.

A cesium dispenser (cesiator) was resistively heated to deliver cesium to the cathode during activation. The rate of cesium dosage could be controlled by the current delivered to the cesiator. The cesiator was mounted on a linear translator so that during activation the device could be placed very near the surface of the cathode and retracted afterwards to avoid blocking any of the illumination or collection a portion of the photocurrent on the cesiator. Furthermore, a small bias voltage was applied to the cesiator as a further means of preventing photoemitted electrons from collecting on the cesiator.

The oxidizing agent was kept in an external manifold and was introduced to the chamber through a precision leak valve. The opening of the valve was directed at the cathode, as shown in Figure 2.

Also mounted to the chamber was a hydrogen cracker that could be used to deliver atomic hydrogen to the chamber for the cleaning processes described in the next section.

### *2. System Preparation*

Upon initial installation of a new photocathode in the chamber and after the initial pump-down of the chamber, a thermal bake-out of the chamber was performed using an oven to

remove any residual molecules (mostly water) present due to the exposure of the chamber to atmosphere during the cathode installation. A vacuum level in the low $10^{-10}$ Torr range was achieved after the bake-out. The cathode itself was cleaned by exposing it to atomic hydrogen (produced by the cracker) for 15 minutes. The highly reactive atomic hydrogen is used to form compounds with impurities in the GaAs crystal that are easily removed via heating of the cathode.

Prior to each new activation, the cathode was heat cleaned by bringing the cathode temperature to 650 °C for two hours to desorb surface layers deposited by previous activations as well as other compounds introduced to the system through exposure to the cesiator output and oxidizing gases. Activations were started only after the cathode had cooled to 30 °C after heating. The process of activation was conducted as soon after heat cleaning as possible for consistency between tests.

### *3. Activation Procedure*

Prior to activation, a low current (which does not cause the release of cesium) is passed through the cesiator so as to warm the device to provide a consistent cesium dose during activation. Once ready, the cesiator is position near the cathode and the current is increased to begin depositing the first cesium layer on the cathode surface.

As the first layer is deposited, the QE begins to rise and eventually peaks and begins to decrease as the surface becomes saturated with cesium. Cesium dosing is continued until the QE drops to half of the peak value, at which point the current through the cesiator is reduced to a lower value to stop the deposition of cesium. The leak valve is then immediately opened to expose the cathode to the oxidizer. The rate of exposure is controlled so that the total pressure in the cathode chamber does not exceed $5 \cdot 10^{-8}$ Torr. As exposure begins, QE rises relatively rapidly (depending on the pressure of the oxidizing gas) and peaks, at which instance the leak valve is closed immediately. Over-exposure to the oxidizer leads to a rapid loss in QE that may not be recoverable.

Immediately following the closure of the leak valve, cesiation is restarted and the QE is allowed to peak and fall to half of the peak value again before continuing the cycle with exposure to oxidation. The cycle is repeated until the gain in QE between successive cycles is extremely small. For the activations conducted in this study between 12 and 17 cycles were required to maximize the QE. The activation procedure ends with exposure to the oxidizer. At the end of final oxidizer exposure, the cesiator is retracted away from the cathode. This can lead to a small increase in QE since the cesiator may block part of the laser beam from the cathode or collect part of the photocurrent when in activation position. A typical plot of the evolution of QE during activation is shown in Figure 3.

### *4. Thermal Desorption Analysis*

Following the monitoring of QE decay after activation, the surface composition of the cathode was examined using thermal desorption spectroscopy (TDS). To conduct a TDS test, the photocathode was heated at a rate of 9 °C/min and the resulting desorption from the cathode was monitored using a residual gas analyzer (RGA) to produce a mass spectrum of the compounds desorbing from the surface as a function of temperature. Note that TDS analysis could not be conducted simultaneously with QE measurements since the operation

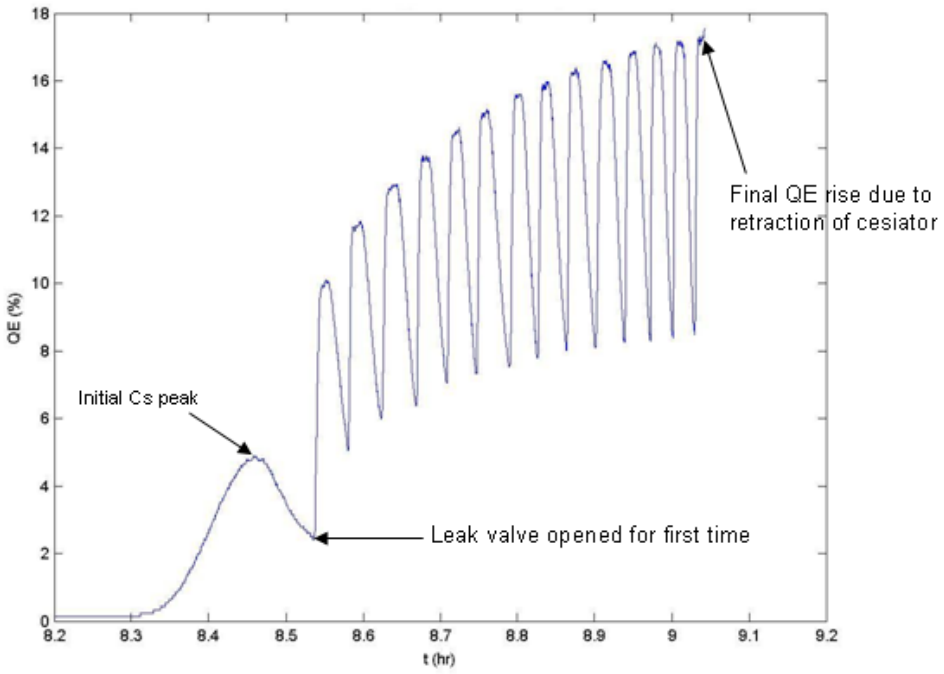


FIG. 3: Time evolution of QE during a typical "yo-yo" activation.

of the RGA leads to spurious effects on the measured QE.

### C. Results of Photocathode Activations

#### 1. *Activations Using $NF_3$*

Nitrogen trifluoride has been shown to be an effective oxidizing agent in the activation GaAs photocathodes, often proving to be easier activate to with than other agents such as oxygen [9]. In this study several activations were attempted using $NF_3$ as the oxidizing agent. While activations using $NF_3$ produced the highest peak QE values achieved in the study, $NF_3$ activations were marked by a sharp initial decline in QE following the activation. A summary of the essential parameters of the $NF_3$ activations which were monitored for decay are presented in Table I. Additionally, several activations were subject to TDS analysis immediately following activation.

In general, photocathodes activated with $NF_3$ exhibited rapid initial decay, as noted by the $1/e$ lifetimes of only a few hours for the majority of tests. The rapid rate of QE decay seen in the first few hours after activation, however, eventually stabilized into a slower decay. This effect can be seen in the decay curves shown in Figure 4. Thus, low QE values are maintained for extended periods of time after the initial high QE value decays. It was found in long-term decays that eventually the instantaneous lifetime of the cathode after several hours of decay grows to exceed 50 hours. This behavior is discussed in more detail in later sections.

Thermal desorption analysis of cathodes activated using $NF_3$ showed two notable features.

| Test Date | Max QE (%) | # Cycles | Initial QE (%) | Lifetime (hr) | Notes |
|---|---|---|---|---|---|
| 6-19 | 18.0 | 17 | 6.1 | 9.64 | Long-term decay |
| 6-22 | 12.5 | 15 | 5.9 | 2.55 | $NF_3$ overdose |
| 6-23 | 17.5 | 16 | 6.0 | 3.40 | |
| 6-24 | 17.4 | 19 | 5.6 | 5.74 | |
| 6-25 | 16.8 | 18 | 5.6 | 3.47 | |
| 6-26 | 17.0 | 18 | 5.2 | 3.89 | Long-term decay |
| 7-1 | 17.4 | 15 | 5.2 | 3.92 | Decay data unavailable |
| 7-30 | 11.7 | 16 | 3.2 | N/A | Decay data unavailable |

TABLE I: Summary of activation conducted using $NF_3$ as the oxidizing agent. "# Cycles" refers to the number of cesiation/oxidation cycles conducted during the activation, "Initial QE" refers to the QE achieved from the initial cesiation alone, and "Lifetime" refers to the simple $1/e$ (36.8%) lifetime of the QE decay from the maximum achieved value. All test dates are M-D-2009.

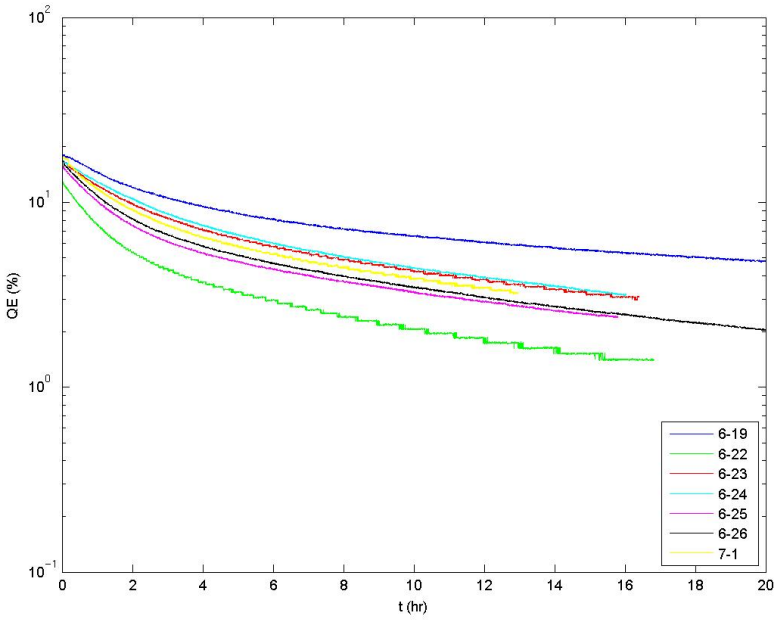


FIG. 4: Decay of QE following activations using $NF_3$ as the oxidizing agent. Time 0 corresponds to the end of activation.

First, the spectra exhibited consistent signals (independent of temperature) at mass numbers 33, 52, and 71 corresponding to the characteristic spectrum peaks of $NF_3$. The cause of this effect was determined to be due to leaking of $NF_3$ from the manifold even when the leak valve was believed to be completely shut. The small extra dose of oxidizer caused by this leak may be responsible for the rapid initial decay of the QE of the $NF_3$ activations, however, more tests are necessary to confirm this.

The second notable feature of the TDS data from $NF_3$ activations was the significant amount of nitrogen and ammonia found to desorb from the cathode upon heating. The mass spectrum from the 6-29 test is shown in Figure 5, demonstrating clear temperature

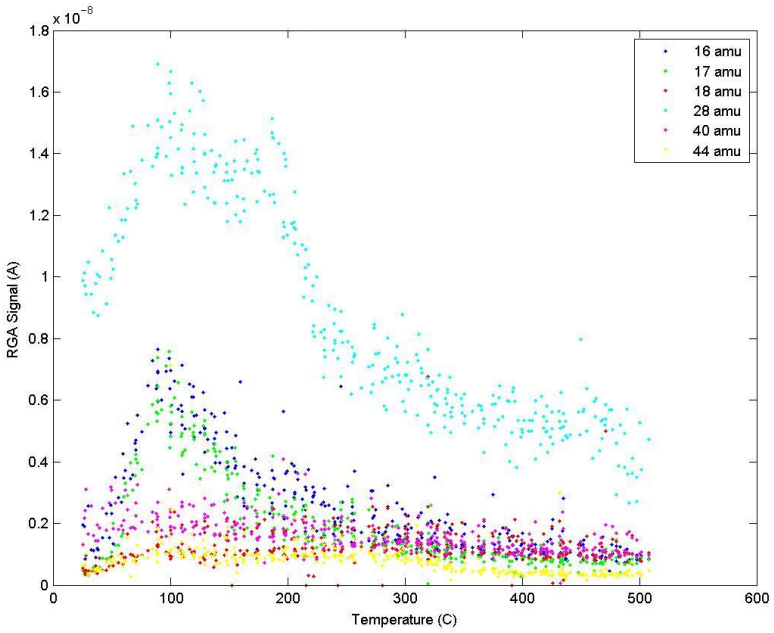


FIG. 5: Trends of the notable mass numbers for the thermal desorption test following a typical $NF_3$ activation.

dependent behavior for the 16 and 17 mass numbers corresponding to ammonia and the 28 mass number corresponding to molecular nitrogen. While most of the activity at 28 amu is likely due to the presence of CO in the system, the behavior of the spectrum at 14 amu suggests that the peak behavior seen for 28 amu is due to nitrogen desorption. It has been found previously via synchrotron radiation photoelectron spectroscopy that significant amounts of nitrogenous compounds are present in the activation layers following activation with $NF_3$ [9], and the TDS data from this study further supports this finding. The presence of ammonia and/or nitrogen in the activation layers indicates that the simple model of layers of Cs-F dipoles on the cathode surface does not completely describe the cathode surface, and hence more complicated surface chemistry must be considered to accurately model the surface behavior.

### *2. Activations Using $XeF_2$*

Following the finding of the presence of significant amounts of nitrogen in the activation layers after activation with $NF_3$ it was proposed to attempt a new method of activation using xenon difluoride as the oxidizing compound. It was hypothesized that upon reaction with the surface, $XeF_2$ would deposit fluorine in the activation layers and release the noble gas Xe into the chamber which would not deposit on the cathode and complicate the surface chemistry. Xenon difluoride exists a crystalline solid with a vapor pressure of about 4 Torr at room temperature [11]. The $XeF_2$ was purchased commercially packed under helium gas, which would provide a means of delivering $XeF_2$ to the cathode by the same methods used for other oxidizing gases. After the initial $XeF_2$ tests, however, it was determined that a significant amount of nitrogen (one part in seven) was present in the packing gas of the $XeF_2$.

| Test Date | Max QE (%) | # Cycles | Initial QE (%) | Lifetime (hr) | Notes |
|---|---|---|---|---|---|
| 7-6 | 15.9 | 13 | 5.4 | N/A | No purification |
| 7-8 | 14.9 | 11 | 4.7 | N/A | ” |
| 7-10 | 14.6 | 15 | 4.5 | 30.8 | ”, Lifetime estimated by fit |
| 7-14 | 13.7 | 12 | 4.7 | 3.61 | One purification |
| 7-15 | 11.7 | 15 | 4.0 | 4.54 | ” |
| 7-20 | 12.2 | 14 | 4.0 | N/A | Two purifications, short decay |
| 7-21 | 12.3 | 14 | 4.0 | 16.1 | ” |
| 7-24 | 11.0 | 14 | 3.2 | 16.4 | ”, long-term decay |
| 7-29 | 9.66 | 13 | 3.3 | N/A | Three purifications, short decay |

TABLE II: Summary of activation conducted using $XeF_2$ as the oxidizing agent. “# Cycles” refers to the number of cesiation/oxidation cycles conducted during the activation, “Initial QE” refers to the QE achieved from the initial cesiation alone, and “Lifetime” refers to the simple $1/e$ (36.8%) lifetime of the QE decay from the maximum achieved value, which was not available for tests not allowed to decay that far. All test dates are M-D-2009.

A series of purifications of the packing gas was conducted to reduce the level of nitrogen in the packing gas to less than one part in 4000. Unique decay behaviors were found for activations following each successive purification.

The purification process of the $XeF_2$ packing gas consisted of first cooling the $XeF_2$ bottle to approximately -20 °C using a salt water ice bath. By cooling the bottle to this temperature, the vapor pressure of $XeF_2$ was lowered to approximate $10^{-5}$ Torr to minimize the loss of $XeF_2$ in the purification process. Once cooled, a turbo-pump was used to remove the packing gas from the bottle. The bottle was then backfilled with pure helium. The process of pumping-down and backfilling was repeated several times to remove as much nitrogen as possible from the bottle.

A summary of the key parameters of the $XeF_2$ activations is presented in Table II. Note that several of the tests do not have available values for the simple $1/e$ lifetime since the decay monitoring periods were too short for the QE to decay to that point due to the longer lifetimes exhibited by the $XeF_2$ tests. The lifetime behaviors of the various $XeF_2$ will be further addressed.

As noted, the decay behaviors seen after activations following the various purifications showed unique trends. The trends for several of the $XeF_2$ tests representative of the decays for different states of purification are shown in Figure 6. As can be seen, the most stable QE decay with the longest measured lifetimes occurred for activations using the $XeF_2$ as purchased, packed in a combination of nitrogen and helium. In these initial tests, the QE did not exhibit the usual initial sharp decay and instead immediately began the more stable exponential decay typical of other activations a few hours after the initial drop. The reason for this behavior is unknown, but could be due to the presence of other compounds (including nitrogen) in the original packing gas that led to a different cathode surface structure than created in other activations.

The discovery of nitrogen in the system, including ammonia as will be discussed, led to attempts to replace the $XeF_2$ packing gas with pure helium. After the first purification attempt, the nitrogen level in the $XeF_2$ packing was reduced to approximately 1/70 of the packing gas total pressure. The decays seen after one purification were the fastest observed

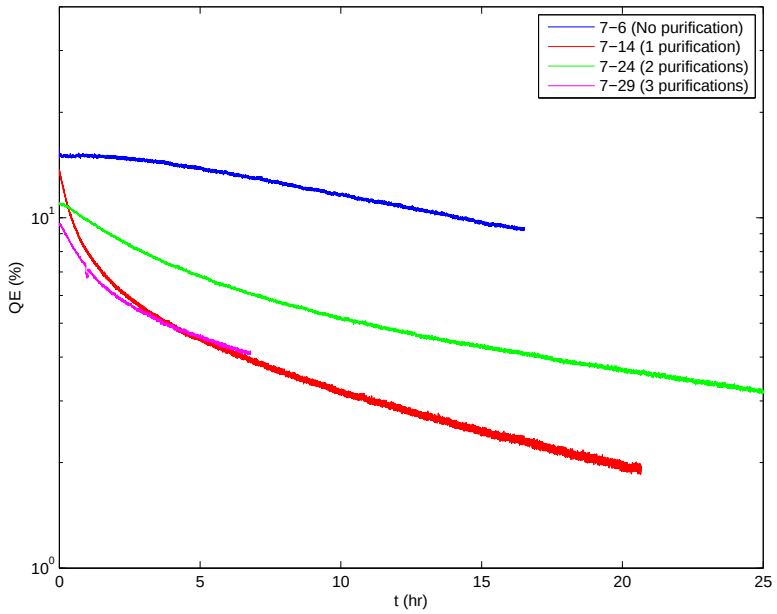


FIG. 6: Plot of the time evolution of QE after activation for several $XeF_2$ activations, representative of the decay behavior after successive purification attempts. Time zero corresponds to the end of activation.

for $XeF_2$ activations, but were still slower than decays following $NF_3$ activations. The stability of the cathode was improved by a second purification, which led to a shallower initial decay and eventual long in the long-term decay.[1]

Analysis of the cathodes activated with $XeF_2$ using TDS produced surprising results in that, even after successive purifications of the packing gas, the presence of ammonia in the system could not be eliminated. As is seen in Figure 7, after two purifications peaks at mass numbers 16 and 17 still occurred near 105 °C, indicating the desorption of ammonia from the system at the same temperature at which ammonia was found to desorb in the $NF_3$ tests. It should be noted that the peak of mass numbers 16 and 17 is only approximately 1/4 the size of the peak seen for $NF_3$ tests and that the magnitude of the 28 amu signal is also significantly reduced, indicating that less nitrogen is present in the $XeF_2$ activation systems. After two purifications, however, it was found that successive purifications did not reduce the size of the ammonia peak, indicating that a source of nitrogen other than the oxidizing gas and its packing existed in the system. Possible sources of nitrogen in the system and its role in the activation and stability of the photocathode will be discussed in the next section.

[1] It should be noted that only one activation was conducted after the third purification in this study, and thus more tests (such as monitoring of long-term decay behavior) are necessary to fully characterize the decay behavior. The decay observed for this single test is included in Figure 6 for completeness.

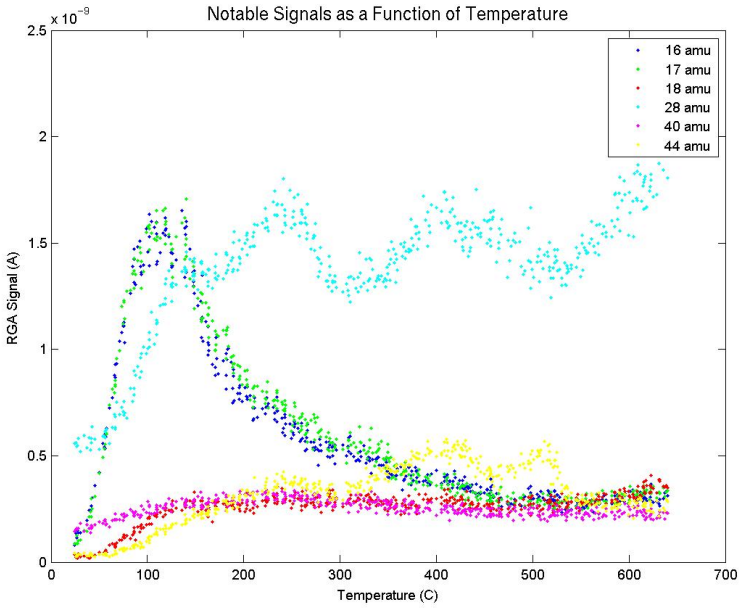


FIG. 7: Trends of the notable mass numbers for the TDS analysis of the heat cleaning following the 7-21 activation (2 purifications).

### D. Long-Term Decay Behavior

Several tests were conducted to determine the decay behavior of the QE of activated photocathodes at long times ($>$ 10 hours after activation). It was found that regardless of the oxidizing agent used ($NF_3$ or $XeF_2$) that distinct change in the decay behavior occurred between 10 and 20 hours after activation, depending on the test. Figure 8 shows the evolution of the "instantaneous' lifetime of the QE for the long-term tests after activation. In this case the instantaneous lifetime was calculated by applying an exponential fit to small segments of the data in the vicinity of successive points in time to determine the rate of decay at that time.

As can be seen, each of the tests shows approximately rapidly increasing lifetime immediately following activation, but that then the increasing of the lifetime stabilizes. In the case of the 6-19 and 7-24 tests, the lifetime plateaus at a high (approximately 50 hours) constant value characteristic of a pure exponential decay. While the 6-26 did not exhibit a leveling-off of the lifetime, it did exhibit a marked change in the rate of change of the lifetime around 10 hours after activation. The various short term tests conducted confirmed the observed behavior of a rapid, linear increase in instantaneous lifetime immediately following activation.

It is notable that the eventual instantaneous lifetimes achieved by the $NF_3$ and $XeF_2$ tests are very comparable, suggesting that a process independent of the oxidizing compound used dominates the effects seen in long-term QE decay. Note that $XeF_2$ activations maintained higher QE for longer periods of time, and thus had higher simple $1/e$ lifetime values since $XeF_2$ tests tended to start with higher instantaneous lifetimes, indicative of the absence of the rapid initial decay seen in $NF_3$ tests.

It seems likely that the "turning-point" in decay behavior common to each of the long-

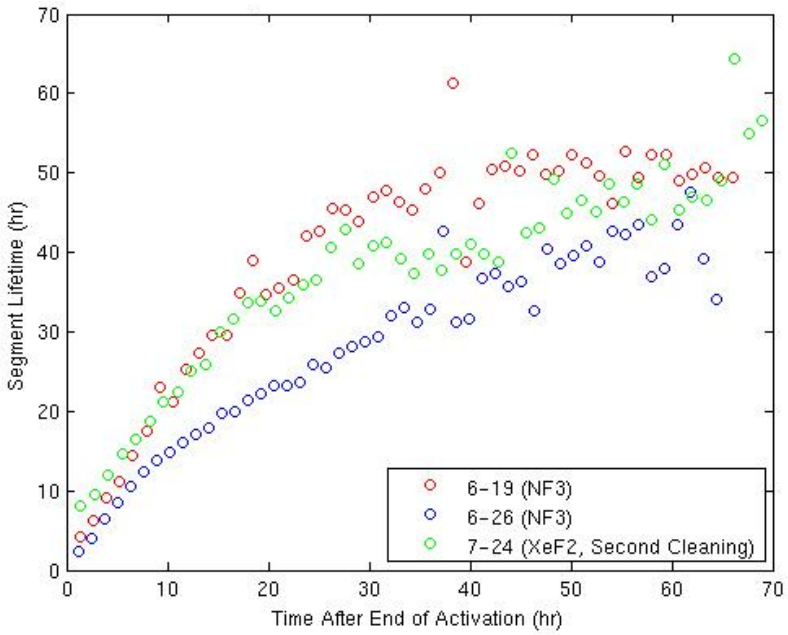


FIG. 8: Evolution of the instantaneous (segment) lifetimes of the long-term QE decay tests after activation.

term tests is related to the depletion of some compound from the cathode or chamber or another fundamental change in the cathode activation layers. If the cause of this behavior could be identified, it may be possible to prepare a cathode in such a way to avoid the initial behavior following activation to produce cathodes that immediately achieve high, stable lifetimes.

### E. Nitrogen in the Activation and Decay Processes

As noted, nitrogen was found to be present in activations using both $NF_3$ and purified $XeF_2$, at least partially in the form of ammonia which was consistently found after activations. Furthermore, smaller ammonia peaks also appeared when TDS analysis was conducted on a cathode that had been exposed to only the cesiator output and with no exposure to any outside agents. This suggests that the integrity of the chamber vacuum and the purity of the cesiator output may not be of sufficient quality to guarantee that only cesium and the desired oxidizing agent participate in the formation of the activation layers on the photocathode. Extensive leak testing of the cathode chamber found no evidence of leaks to atmosphere, which is also suggested by the fact that no evidence of oxygen was present in any of the TDS tests conducted. Systematic studies of these issues will continue in future work.

#### *1. Effects of Nitrogen on Activation*

To explore the effect of the presence of nitrogen on the activation process an activation was attempted using pure molecular nitrogen as the oxidizing agent to determine whether

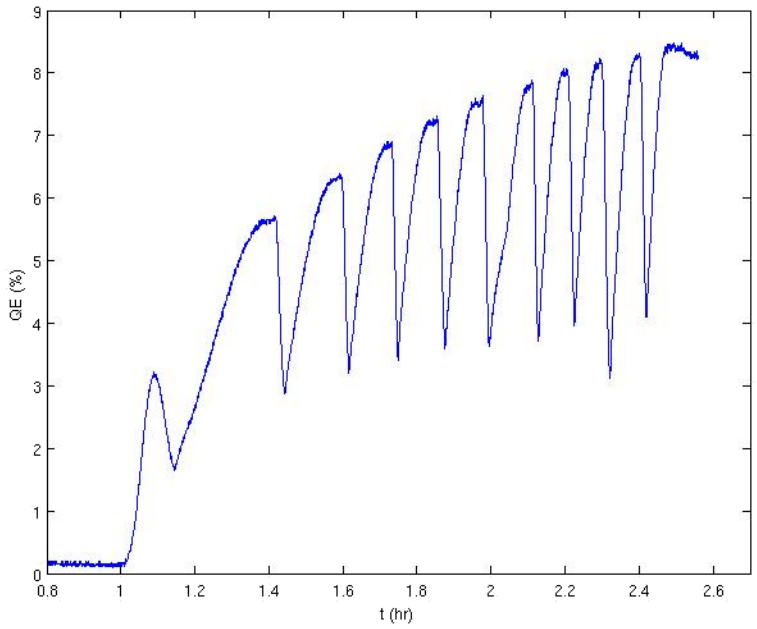


FIG. 9: Evolution of QE during the activation attempt using pure nitrogen as the oxidizer.

or not a cathode could be activated in this fashion. It was found that, indeed, a GaAs photocathode can be activated using the "yo-yo" method, alternating deposition of cesium with exposure to $N_2$. The evolution of QE during the activation is shown in Figure 9. While the QE achieved (8.5%) was somewhat lower than that achieved using the other activation methods for similar initial QE values (from the first cesiation only), it is clear that the cathode was successfully activated via exposure to $N_2$. The decay of the $N_2$ activation was not studied for long-term behavior, which will be a subject of future studies.

The result of this test further suggests that nitrogen may play a significant role in the formation of cathode activation layers. Further studies on the activation and decay behavior resulting from pure $N_2$ exposure would be valuable in future work.

### *2. Annealing of the Cathode to Remove Ammonia*

A second procedure used to study the effect of nitrogen and nitrogen compounds on the cathode surface consisted of "annealing" the cathode by heating to the temperature of ammonia desorption (100-105 °C) at the rate used in the TDS analyses (9 °C/min) during the QE decay after activation in attempt to remove ammonia from the surface. It was shown that as the cathode is heated a slight decrease in QE occurs (as would be expected from the destabilization of the surface layers) but that the QE increases significantly as the temperature approaches and holds at the temperature of peak ammonia desorption. The temperature was held at the peak desorption temperature until no further increase in QE was occurring, and then the cathode was allowed to cool. During the cooling, a further increase in QE occurred. The QE versus temperature plots for the anneal attempts are shown in Figure 10.

In the case of both anneals, the QE after re-cooling is 10-20% greater than the QE prior

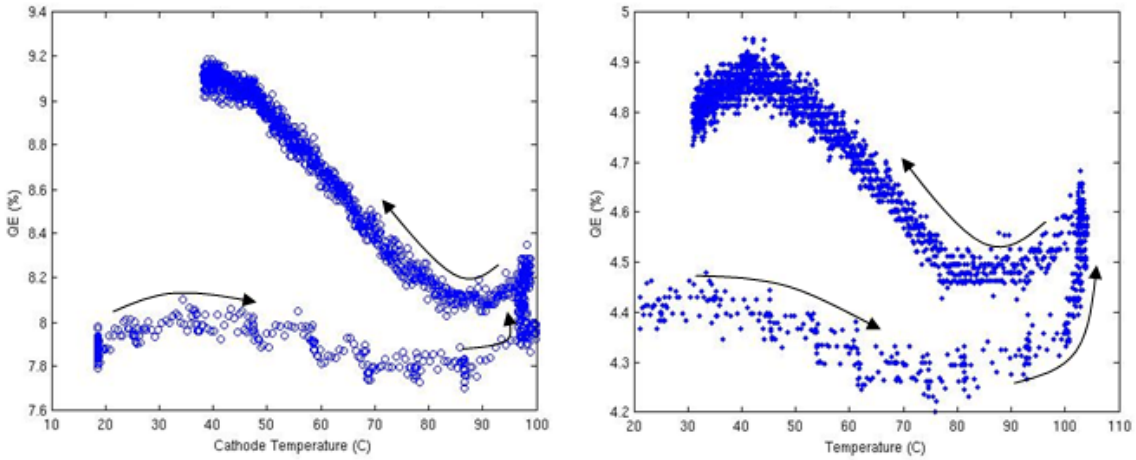


FIG. 10: Results of the two cathode anneal attempts (left: 7-8, right: 7-22), plotting QE versus cathode temperature. The arrows indicate the direction of time progression in the tests.

to the beginning of the annealing process. It appears that the recovery of QE corresponds to the desorption of ammonia from the cathode, since no other compounds were found to desorb in significant quantities from the cathode at the same temperature. The QE decay after annealing, however, is much more rapid than the decay before the anneal, likely due to the destabilization of the activation layers caused by the heating.

It is necessary to confirm that the QE recovery is indeed due to desorption of ammonia. Such a confirmation would shed light on the role of nitrogen and its compounds in cathode activations.

### F. Conclusions

It was shown that $XeF_2$ may be used as the oxidizing agent to successfully activate GaAs photocathodes and preliminary tests suggest that $XeF_2$ may be more stable in the period immediately following activation. To confirm that $XeF_2$ produces activated cathodes with longer lifetimes than $NF_3$, it will be required to further study both activation types in a more controlled environment to avoid aforementioned factors that may have affected the lifetime measurements in this study. The stability of QE decay at long times after activation combined with the lack of initial sharp decline in QE observed for $XeF_2$ produced activations with longer lifetimes than achievable for $NF_3$ activations, although the lifetimes still do not satisfy the long-term goals for cathode stability (lifetimes on the order of hundreds or thousands of hours). Furthermore, the consistent presence of nitrogen in the cathode system presents a challenge to understanding the processes governing photocathode activation and QE decay.

Future work will continue to focus on developing stable, long-lasting photocathodes and understanding the source and effect of nitrogen in the cathode system. As part of these studies, it would be extremely beneficial to develop a method to simultaneously conduct TDS analysis while monitoring QE. Such ability would be advantageous in determining the cause of the observed "turning-point" behavior in long-term QE decays as well as understanding the processes involved with tests such as the cathode anneals. It would also be of interest to

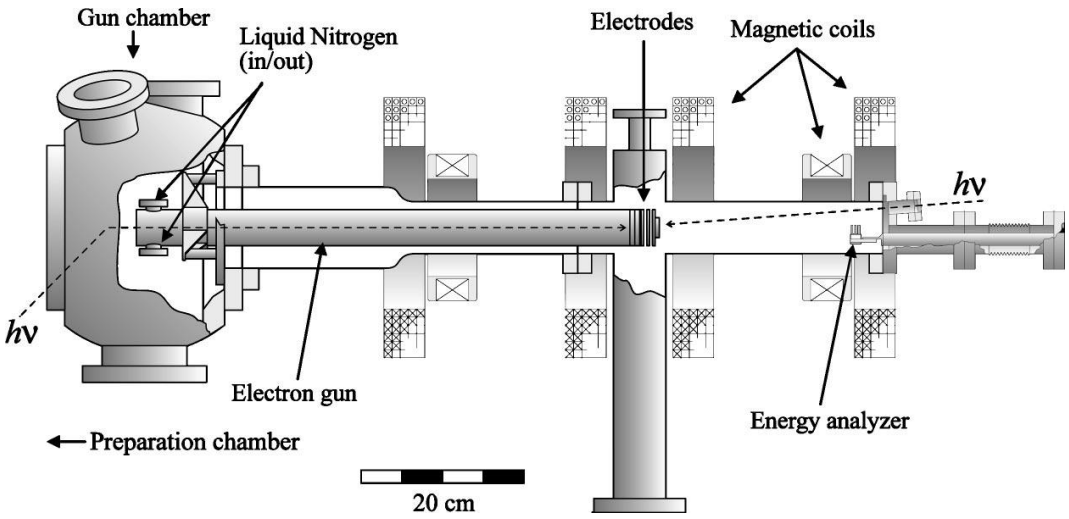


FIG. 11: Schematic of the device built by Hoppe, et al for the measurement of 2D energy distributions of photoelectrons [3].

compare the activations conducted in this study with activation using $O_2$, another commonly used oxidizing agent for GaAs cathode activation, in future studies.

## III. DESIGN OF ENERGY DISTRIBUTION MEASUREMENT DEVICE

The second portion of the study consisted of preliminary work in designing an apparatus for the measurement of the two dimensional energy distributions of electrons emitted from photocathodes for future construction at Cornell University. The preliminary work followed the design of a device developed at the University of Heidelberg by Hoppe, Weigel, and others [2, 3]. The design developed at the University of Heidelberg showed promising initial results in terms of capability to effectively measure both dimensions of the electron energy distribution simultaneously and the design at Cornell will seek to improve upon their model.

The device designed by Hoppe, et al depends on the use of a retarding field analyzer (RFA) placed in line with the electron beam to very sensitively measure the longitudinal energies of photoelectrons. The RFA is set to a specific retarding potential and repels all electrons with energies less than that potential. Electrons with higher energies than the potential are collected behind the retarding electrode and measured as a current. By scanning the retarding potential over the range of electron energies the complete longitudinal distribution of energies may be obtained [5].

The transverse energy distribution is then computed from the longitudinal distribution making use of the adiabatic invariance of the magnetic moment of electrons provided that the electrons are not exposed to a magnetic field that changes rapidly relative to the size of the cyclotron spirals of the electrons in the magnetic field, as described in the next section. Electrons are accelerated away from the cathode by a series of electrodes that may be set to varying potentials to accelerate the electrons to greater velocities and to extract electrons only of certain energies. A schematic of the device constructed by Hoppe, et al is shown in Figure 11.

A brief discussion of the essential function of the device and a summary of the work to date is provided in the following sections. For more a more detailed discussion of the device,

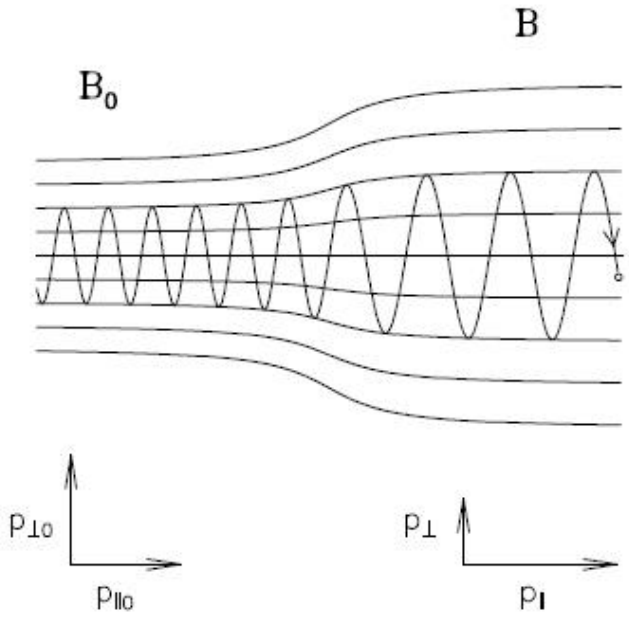


FIG. 12: Simplified trajectory of an electron in a strong longitudinal magnetic field [3].

consult the cited theses by Weigel and Hoppe.

### A. Theory

An electron traveling through a static magnetic field that changes slowly in space will tend to follow magnetic field lines with a spiraling trajectory about that field line [12]. The device designed by Hoppe, et al is immersed in a strong static magnetic field to guide electrons to the RFA. Furthermore, the strength of this field can be varied longitudinally across the device to affect the nature of the trajectories of the electrons, as shown in the illustration of Figure 12. Since the only significant forces experience by the electrons as they travel from the accelerating electrodes to the RFA is the magnetic field which performs no work and the electric potential is constant outside of the electrode regions, it may be taken that the kinetic energy of the electrons is conserved while in transit.

To allow the simultaneous measurement of both the transverse and longitudinal energies, the device developed by Hoppe, et al utilizes the fact that if an electron passes through a magnetic field which changes slowly in space with respect to the cyclotron radius and helix spacing of the electron's trajectory then the magnetic moment of the electron is approximately invariant. The magnetic moment under such conditions is known as the "first adiabatic invariant"; adiabatic referring to the condition of slowly changing magnetic fields. The magnetic moment of the electron may be expressed as:

$$\mu = \frac{E_\perp}{B} \approx \text{constant} \tag{2}$$

where $E_\perp$ is the transverse component of the kinetic energy of the electron and $B$ the magnitude of the axial magnetic field. The conservation of the kinetic energy of the electron

in transit across the device may be expressed as:

$$E_\perp + E_\parallel = \text{constant} \tag{3}$$

where $E_\parallel$ is the longitudinal kinetic energy of the electron. Then if the ratio of the magnetic field strength at the RFA $B_f$ to the magnetic field strength at the cathode $B_i$ is defined to be $\alpha$, then by use of the adiabatic invariant the transverse and longitudinal energies at the RFA ($E_{\perp f}$ and $E_{\parallel f}$) may be expressed in terms of the energy distributions at the cathode ($E_{\perp i}$ and $E_{\parallel i}$) by:

$$E_{\perp f} = \alpha E_{\perp i} \tag{4}$$

$$E_{\parallel f} = E_{\parallel i} + (1-\alpha)E_{\perp i} \tag{5}$$

Hence from Equation 5 it immediately follows that:

$$E_{\perp i} = -\frac{dE_{\parallel f}}{d\alpha} \tag{6}$$

Therefore, by varying the ratio of field strengths $\alpha$ and utilizing the RFA to measure the final longitudinal energy, the transverse energy distribution at the point of emission may be computed. The longitudinal energies at emission may then be computed from Equations 4 and 5 to yield the 2D energy distribution of the electrons [5].

### B. Progress to Date

During the course of this study the preliminary work on creating a similar device consisted of creating electromagnetic field maps for the essential components of the device, including the accelerating electrodes, the RFA, and coils used to create the axial magnetic field. The field mappings were created using the program *Poisson Superfish* developed at Los Alamos National Laboratory [13].

The Poisson Superfish input files as well as preliminary generation of the field maps are not provided here due to space considerations. See the appendix on how to obtain these files. The input files are commented so as to highlight the various elements of the device geometry.

### C. Future Work

Future work will entail utilizing the field maps created in this study to simulate the passage of electrons through the device and to identify necessary areas of improvement and refinement of the Hoppe, et al design. One area for improvement will be altering the geometry of the retarding electrode in the RFA to ensure that all electrons experience the same retarding potential regardless of their radial position in the beam. This issue is discussed in detail in the Hoppe thesis [3]. Naturally, the ultimate goal is to construct the device and utilize it to make detailed measurements of electron energy distributions of photocathodes. These measurements would be an extremely useful tool in comparing different activation methods and better understanding the surface interactions responsible for activation.

## IV. ACKNOWLEDGEMENTS

Many thanks to my advisors Dr. Ivan Bazarov, Dr. Yulin Li, and Dr. Xianghong Liu of Cornell University who proposed my projects for this research experience and skillfully guided me through learning the necessary background material and how to operate the various aspects of the experimental setup. I would also like to acknowledge Dr. John Dobbins for providing assistance in setting-up an automatic controller for the illumination laser on the experimental setup. Thanks also to those whose efforts made the REU program possible including Rich Galik, Ernie Fontes, Lora Hines, Monica Wesley, and others. This work was supported by the National Science Foundation REU grant PHY-0849885.

## V. APPENDIX: ARCHIVE OF DATA FILES AND FIELD MAPS

Refer to `http:\\lepp.cornell.edu\~ib38\reu\09\Henderson` for the archive of data files, *Poisson Superfish* input files, field maps, as well as copies of this report and presentations associated with this work. Consult the README file in the top directory of the archive for a listing/description of the archive contents.

---

[1] H.J. Drouhin, C. Hermann, and G. Lampel. Phys. Rev. B **31**, 3859 (1885).
[2] U. Weigel. PhD dissertation, Universität Heidelberg, 2003. 7.
[3] M. Hoppe. PhD dissertation, Universität Heidelberg, 2001. 8.
[4] I.V. Bazarov, B.M. Dunham, and C.K. Sinclair. Phys. Rev. Lett. **102**, 104801 (2009).
[5] D.A. Orlov, M. Hoppe, U. Weigel, D. Schwalm, A.S. Terekhov, and A. Wolf. Appl. Phys. Lett. **78**, 2721 (2001)
[6] W.E. Spicer and A. Herrera-Gómez. SLAC-PUB-6306 (1993).
[7] J.J. Scheer and J. van Laar. Solid State Commun. **3**, 189 (1965).
[8] T. Maruyama, D.-A. Luh, A. Brachmann, J.E. Clendenin. E.L. Garwin, S. Harvey, J. Jiang, R.E. Kirby, and C.Y. Prescott. Appl. Phys. Lett. **85**, 2640 (2004).
[9] Z. Liu, Y. Sun, S. Peterson, and P. Pianetta. Appl. Phys. Lett. **92**, 241107 (2008)
[10] S. Pastuszka, M. Hoppe. D. Kratzmann, D. Schwalm, and A. Wolf. J. Appl. Phys. **88**, 6788 (2000).
[11] V.M. Bermudez. Appl. Surf. Sci. **119**, 147 (1997).
[12] T.G. Northrop. Ann. Physics **15**, 79 (1961).
[13] *Poisson Superfish.* Available: `http://laacg1.lanl.gov/laacg/services/download_sf.phtml`